High Power Laser Science and Engineering, (2025), Vol. 13, e53, 10 pages.
doi:10.1017/hpl.2025.10032

HIGH POWER LASER SCIENCE AND ENGINEERING

RESEARCH ARTICLE

A B-integral management strategy in discrete single-crystal fibers: towards direct power scaling of femtosecond sources near 2 μm

Jianlei Wang[1,3], Yongguang Zhao[1], Ning Zhang[2], Wenlong Wei[2], Chun Wang[3], Haohai Yu[1], Valentin Petrov[4], and Huaijin Zhang[1]

[1]*State Key Laboratory of Crystal Materials and Institute of Crystal Materials, Shandong University, Jinan, China*

[2]*Jiangsu Key Laboratory of Advanced Laser Materials and Devices, School of Physics and Electronic Engineering, Jiangsu Normal University, Xuzhou, China*

[3]*Key Laboratory of Laser & Infrared System, Ministry of Education, Shandong University, Qingdao, China*

[4]*Max Born Institute for Nonlinear Optics and Short Pulse Spectroscopy, Berlin, Germany*

(Received 22 January 2025; revised 7 April 2025; accepted 29 April 2025)

Abstract

We propose a B-integral management strategy for manipulating the nonlinear effects by employing a discrete single-crystal fiber (SCF) configuration, enabling direct amplification of 2-μm femtosecond pulses at high repetition rates without additional pulse picking, stretching and compression. The system delivers an average power of more than 56 W at 75.45 MHz with extremely high extraction efficiency (>55%) and near-diffraction-limited beam quality ($M^2 < 1.2$). The dynamic evolution of the optical spectra and temporal properties in the power amplifier reveals that detrimental nonlinear effects are largely suppressed due to the low accumulated nonlinear phase shift in the discrete SCF layout. This straightforward, compact and relatively simple approach is expected to open a new route to the amplification of 2-μm ultrashort pulses at MHz and kHz repetition rates to achieve high average/peak powers, thereby offering exciting prospects for applications in modern nonlinear photonics.

Keywords: chirp-free amplification; femtosecond pulses; near-diffraction-limited beams; single-crystal fiber; ultrafast amplifier

1. Introduction

High average/peak power ultrafast lasers in the 2-μm spectral range have attracted considerable interest due to numerous scientific and industrial applications, for example, laser-driven compact soft X-ray sources through high-order harmonic generation (HHG) with the driving wavelength located at the 'sweet spot' for pushing the phase-matched harmonic energy beyond the carbon K-edge[1,2], next-generation laser-driven electron/positron colliders based on the recently proposed big aperture thulium (BAT) laser concept with high true wall-plug efficiency[3], efficient pump sources for generating mid-infrared radiation via frequency down conversion in non-oxide optical crystals that exhibit high nonlinearity but a lower bandgap, which prevents pumping at 0.8–1 μm[4], and light sources, in particular at high repetition rates for the high accuracy and high signal-to-noise ratio (SNR) of greenhouse gas detection, and high-precision micromachining of transparent organic materials relying on direct linear absorption of the incident photons[5,6]. The generation of ultrashort pulses in the femtosecond regime primarily relies on mode-locking of lasers in a relatively high-quality-factor cavity, which limits the power scalability due to the inevitable trade-off between the pulse duration and the output average power[7]. Therefore, the amplification of ultrafast lasers in the 2-μm spectral range towards high average/peak power has seen rapid development in the past decade[8–10].

The large B-integral, that is, the strong nonlinear phase shift during the amplification process, severely limits the power-handling capability, making direct amplification of femtosecond pulses towards high average power

Correspondence to: Y. Zhao and H. Yu, State Key Laboratory of Crystal Materials and Institute of Crystal Materials, Shandong University, Jinan 250100, China. Emails: yongguangzhao@yeah.net (Y. Zhao); haohaiyu@sdu.edu.cn (H. Yu). C. Wang, Key Laboratory of Laser & Infrared System, Ministry of Education, Shandong University, Qingdao 266237, China. Email: chunwang@sdu.edu.cn

difficult[11,12], and it appears to be limited only in the picosecond regime for both conventional bulk and fiber amplifiers operating in the 2-μm spectral range[8,10]. Thus, the chirped-pulse amplification (CPA)[13] system based on pulse stretching and compression is commonly required. To date, femtosecond amplifiers at 2 μm can be categorized into two main approaches both based on CPA technology, that is, optical parametric chirped-pulse amplification (OPCPA) in nonlinear crystals[14] and laser CPA in Tm- or Ho-doped gain media[15,16].

Broadband amplification achievable in multi-stage OPCPA systems enables few-cycle pulse generation with multi-mJ pulse energies at kHz repetition rates[17–20], with the resulting multi-tens of GW peak powers capable of high-flux soft X-ray HHG[17]. The downside of such systems is the limited average power due to thermal effects and the relatively low efficiency. In addition, synchronized high-energy picosecond pulses are required from a pump source, which inevitably increases the complexity and cost[21,22]. Fiber-based CPA systems are less prone to thermal and thermo-optical effects, making their average power scaling with high beam quality more feasible, but the output energy/peak power is restricted by unwanted nonlinear effects and optical damage[23,24]. Photonic-crystal fibers (PCFs)[25-27] or large-pitch fibers (LPFs)[28-30] can partially overcome these problems and improve the peak power to the GW level[31], but their design and fabrication remain technically challenging. Regarding the nonlinear effects and in particular the self-focusing limitation for further peak power scaling, coherent beam combining offers a promising new direction for such fiber-based CPA systems[32]. In comparison, energetic pulses (multi-tens of mJ) with high peak power exceeding 10 GW can be achieved employing bulk Tm/Ho crystalline regenerative CPA systems[33,34], but the repetition rate is restricted to a few kHz and thermal effects come into play as in the OPCPA system. Thus, achieving high pulse energies at high repetition rates, that is, high average powers in the 2-μm spectral range, seems difficult with either of the above-mentioned approaches. In principle, diode-pumped thin-disk and slab geometry amplifiers based on the CPA technique can also be potentially useful for achieving high average power together with high pulse energy, as demonstrated in the 1-μm spectral range[35,36]; however, these laser designs are relatively complex to implement near 2-μm[37], which is related to material availability, doping level restrictions and the lower laser gain. As a consequence, such multi-pass geometries require many more passes and greater effort for beam shaping at 2 μm.

In summary, the direct amplification system features simplicity and a compact structure, but exhibits poor power-handling capability of the watts level limited by the strong nonlinear phase shift of the femtosecond pulses, and the CPA system is now the preferred method but also remains challenging in the 2-μm spectral range for all bulk systems (OPCPA), regenerative amplifiers and thin-disk and slab amplifiers due to their inherent technical difficulties.

Herein, we propose a new strategy to significantly reduce the nonlinear phase shift of the laser beam, allowing direct amplification of femtosecond pulses without stretching or compression. It is also capable of operation at the high repetition rate of the seed oscillator without pulse picking, and delivering a record power from the direct femtosecond amplification systems in the 2-μm spectral range. This strategy is implemented in a compact amplifier system employing a discrete holmium-doped yttrium aluminum garnet (Ho:YAG) single-crystal fiber (SCF) configuration. The term SCF, which is somewhat misleading but already established, refers to a thin crystal rod typically with a diameter of less than 1 mm and a length of a few centimeters[38], that is, it designates an intermediate architecture between bulk crystals and optical fibers. In contrast to optical fibers, it is associated with free-space propagation of the laser beam in combination with wave-guiding of the pump light[39,40]. In the 1-μm spectral range, femtosecond pulses have been amplified to an average power as high as 290 W and a peak power exceeding 2 GW in a simple single-stage SCF amplifier, indicating the inherent capability of SCFs for simultaneous handling of high average and peak powers[41,42]. However, materials near 2 μm typically exhibit anomalous dispersion and a narrower gain spectrum, making it challenging for direct amplification of femtosecond pulses. In this work, by designing a discrete SCF configuration, the accumulated B-integral value can be significantly reduced, thus suppressing the nonlinear effects. As a proof-of-principle study, it shows that a multi-stage SCF amplifier system is capable of straightforward power scaling of 2-μm ultrafast laser sources at high repetition rates with extremely high extraction efficiency and near-diffraction-limited beam quality. The spectral and temporal evolution of the femtosecond pulses in the SCF amplifier is investigated in detail, which will be helpful for future designs of such ultrafast SCF amplification systems towards ultrahigh average and peak powers. The strategy employed here confers direct amplification systems with interesting power scaling prospects and may serve as a good reference for conventional bulk and fiber amplifiers.

2. Design and method

2.1. B-integral management with discrete SCF configuration

Since obtaining high average power femtosecond pulses at a high repetition rate is inevitably accompanied by serious thermal effects in the bulk amplifiers, gain medium doping with a lower concentration of active ions but longer gain region is a straightforward solution. However, the B-integral value (B) will increase in this case due to the continuous

https://doi.org/10.1017/hpl.2025.10032 Published online by Cambridge University Press

accumulation of nonlinear phase shift in the long gain medium (L)[43]:

$$B = \frac{2\pi}{\lambda}\int_0^L n_2(z)I(z)\mathrm{d}z, \tag{1}$$

where n_0 and n_2 are the linear and nonlinear refractive indexes, respectively, λ is the wavelength and I is the beam intensity.

Then, the laser beam starts self-focusing as the peak power exceeds the critical power of $P_{cr} = 3.77\lambda^2/(8\pi n_0 n_2)$[44], thus leading to a reduction of the achievable gain, degraded beam quality and even breakup of the amplified pulses. Although the controllable beam waists of the free-space propagation light in the SCF can mitigate nonlinear effects more effectively than those in conventional silica fibers, the laser performance is still adversely affected when amplifying ultrashort pulses at a high-power level, as demonstrated in the Yb-SCF femtosecond laser amplifier[40].

To overcome this limitation, the strategy employed here is based on a discrete layout of the SCFs, which can provide the following advantages: (i) prevention of continuous accumulation of nonlinear phase shift, that is, discrete B-integral values, and (ii) the length of the SCF is controllable and can be shorter than twice the self-focusing length (Z_f), assuming the average power amplifier reaches P_{max} at the middle of the last-stage SCF amplifier[43]:

$$L < 2Z_f = \frac{2\pi\omega_0^2}{\lambda}\left(\frac{8\pi n_0 n_2 P_{max}}{3\lambda^2} - 1\right)^{-1/2}, \tag{2}$$

where ω_0 is the beam waist radius.

This ensures that the laser pulses exit the SCF before beam collapse, analogous to the multiple-plate structure[44], but with a much lower light intensity in our case. With such a discrete configuration of SCFs (three identical SCFs with 50 mm in length, see the next section for more details), the simulated average power can achieve more than 200 W for 500-fs pulses at a high repetition rate of 50 MHz, with the B-integral value of less than π and $2Z_f$ of approximately 50 mm.

2.2. Experimental setup of the seed source

To perform the direct amplification experiment, Figure 1 schematically shows the entire SCF amplifier system comprising a femtosecond seed source and pre- and multi-stage SCF amplifiers without temporal pulse stretching or compression. The seed source was a wavelength-tunable semiconductor saturable absorber mirror (SESAM) mode-locked Tm(2.8%, atomic fraction):$LuScO_3$ ceramic (3 mm × 3 mm × 3 mm) laser in-band pumped by a home-made continuous-wave (CW) erbium-doped yttrium aluminum garnet (Er:YAG) bulk laser delivering the maximum power of 3.2 W, with a linearly polarized beam at 1645 nm[45]. The pre-amplifier was a Ho:YAG SCF pumped by a laser diode (LD) at 1907 nm, and the main amplifier based on three discrete Ho:YAG SCFs was in-band pumped by a Tm-fiber laser at 1907 nm.

For the seed laser, as shown in Figure 1, the collimated pump beam was focused into the ceramic sample by an aspheric lens (L2, $f = 75$ mm), resulting in a beam diameter of approximately 45 μm. A standard X-shaped astigmatically compensated cavity with a physical length of approximately 2.1 m was employed, in which two plano-concave mirrors, M1 and M2, both with a radius of curvature of $R_{OC} = -100$ mm, formed a beam waist of 30 μm (sagittal) × 60 μm (tangential) diameter within the Tm:$LuScO_3$ ceramic placed at the Brewster's angle between them. Another plano-concave mirror (M3) with $R_{OC} = -150$ mm was used to create a second beam waist of 80 μm in diameter on the GaSb-based SESAM[46] for mode-locking. Two chirped mirrors, CM1 and CM2, providing negative group delay dispersion (GDD) of −125 and −1000 fs^2 per bounce, respectively, were inserted into the other cavity arm for dispersion compensation. This arm was terminated by the output coupler (OC), a plane-wedged mirror with a transmission of $T_{OC} = 3\%$. A home-made 3-mm-thick quartz birefringent filter (BF), cut with its crystal axis at 24° to the surface normal, was inserted close to the OC at Brewster's angle to tune the wavelength of the femtosecond laser for matching the wavelength of the subsequent SCF amplifiers.

2.3. Experimental setup of the direct femtosecond amplification system

After passing through an optical isolator (ISO), the seed pulse was directly imaged into the pre-amplifier via two lenses ($f = 200$ mm). A 1-mm-diameter (Φ), 50-mm-long $Y_3Al_5O_{12}$ (YAG) SCF doped with 0.3% (atomic fraction) Ho^{3+} ions served as a pre-amplifier counter-pumped by a 30 W fiber-coupled LD (400-μm core diameter, 0.22 numerical aperture (NA)) at 1907 nm. The pump light was imaged into the initial part (~3 mm from the pump face) of the SCF using a 1:1 telescope system and then waveguided down to the fiber end through total internal reflection. The pre-amplified femtosecond pulses were directly imaged into the power amplifier, where three identical Ho:YAG SCFs (Φ 1 mm × 50 mm, 0.5% Ho^{3+}) in a serial arrangement with separations of approximately 4 mm were used as gain media. The beam waist with a measured diameter of approximately 460 μm was located in the initial part of the second SCF to ensure free-space propagation of the laser beam in the three-stage SCF power amplifier. A high beam quality (M^2 ~ 1.05) Tm-fiber laser at 1907 nm was employed as a pump source to ensure spatial matching with the beam from the pre-amplifier along the entire SCF power amplifier chain. The pump light

https://doi.org/10.1017/hpl.2025.10032 Published online by Cambridge University Press

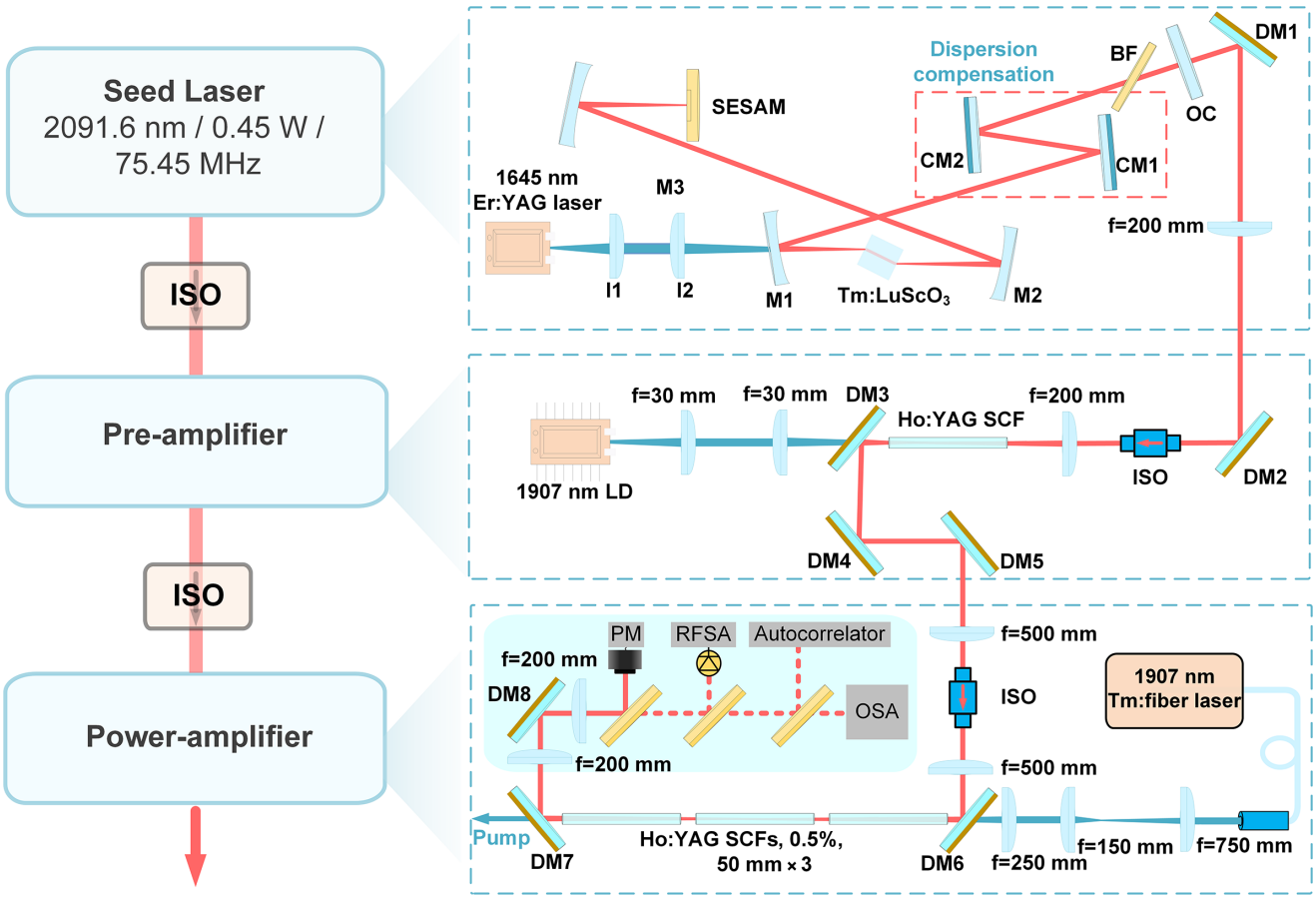

Figure 1. Schematic diagram of the Ho:YAG SCF amplification system. L1/L2, optical collimation/focusing system; M1, M2, M3, concave dichroic mirrors; CM1, CM2, plane dispersive mirrors; OC, output coupler; BF, birefringent filter; DM, plane dichroic mirror; LD, laser diode.

was focused into the second SCF to a spot diameter of approximately 450 μm, with the beam size in the three SCFs not exceeding 600 μm in diameter at any position, thus lengthening the effective gain regions. This makes the experimental setup extremely simple and robust without requiring any re-imaging telescopes. It shall be outlined that all lateral surfaces of the SCFs have been optically polished, and the measured transmission losses were less than 3 dBm^{-1} at 632.8 nm. All input/output SCF faces and all lenses were antireflection-coated. To better mitigate the thermal effects, all the SCFs were mounted in specially designed aluminum modules being in direct contact with cooling water at 13°C.

3. Results and discussion

3.1. Seed source and pre-amplifier systems

The output performance of the mode-locked Tm:$LuScO_3$ laser is shown in Figure 2. For a pump power of approximately 2.5 W, the average output power ranged from 0.24 to 0.35 W when adjusting the intra-cavity BF, corresponding to a tuning spectral span of approximately 63 nm ranging from 2044 to 2107 nm, as shown in Figure 2(a). The autocorrelation traces in Figure 2(b) were recorded by a commercial autocorrelator (APE pulseCheckSM, extended IR), yielding pulse durations (τ) of 195–373 fs.

To match the peak wavelength of the Ho:YAG emission spectrum at approximately 2091 nm, the central wavelength of the seed laser was tuned to 2091.6 nm with a spectral full width at half maximum (FWHM) of approximately 12 nm; see Figure 2(c). The average output power at this wavelength reached 0.45 W at a pump power of 3.2 W, corresponding to a single pulse energy of approximately 6 nJ. The measured autocorrelation trace is presented in Figure 2(d), and the corresponding pulse duration (FWHM intensity) was 360 fs.

Figures 2(e) and 2(f) depict the radio frequency (RF) spectrum of the mode-locked Tm:$LuScO_3$ seed laser at 2091.6 nm. The fundamental beat note at approximately 75.45 MHz exhibited an SNR of more than 65 dBc. The uniform harmonic beat notes observed on a 1 GHz span indicate the absence of spurious modulations and the stable mode-locked operation. The beam quality factor at the maximum average power was $M^2 = 1.01$ and 1.04 in the horizontal (x) and vertical (y) directions, respectively. The inset in Figure 2(d) shows the near-field beam intensity profile, which shows the TEM_{00} mode of the seed laser. The

https://doi.org/10.1017/hpl.2025.10032 Published online by Cambridge University Press

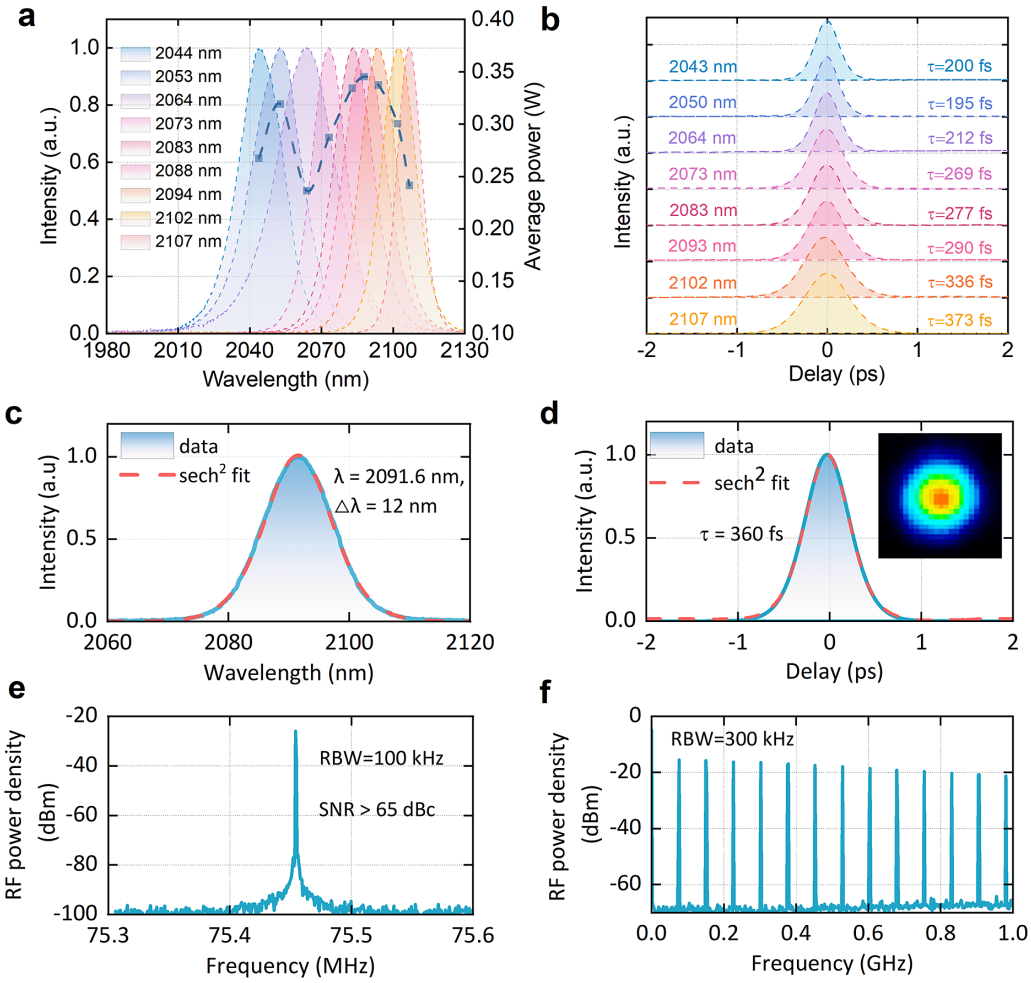

Figure 2. Output performance of the Tm:$LuScO_3$ laser. (a) Tunable mode-locked operation: spectra and average output power (circles and dashed line) and (b) the corresponding autocorrelation traces where τ is the pulse duration (full width at half maximum, FWHM) assuming $sech^2$-temporal shapes. (c) Optical spectrum, (d) autocorrelation trace with the inset showing the recorded near-field spatial beam profile, (e) radio frequency (RF) spectrum of the fundamental beat note measured with a resolution bandwidth (RBW) of 100 kHz and (f) RF spectrum on a 1 GHz span (RBW = 300 kHz) at the selected seed wavelength of 2091.6 nm. SNR, signal-to-noise ratio.

excellent temporal and spatial features are prerequisites for subsequent amplification in the Ho:YAG SCFs.

The Ho:YAG SCF pre-amplifier was designed to increase the average power of the seed laser, and the maximum output power of 0.8 W was reached for an injected seed power of 0.45 W. The amplified pulse spectrum was centered at 2091.5 nm with an FWHM of 10.5 nm (Figure 3(a)), which corresponded to slightly longer pulses of 410 fs (as shown in Figure 3(b)) attributed to the gain narrowing, as well as being slightly affected by material dispersion (see Section 1 in the Supplementary Material for the discussion). The M^2 values measured after the pre-amplifier were only marginally increased, $M_x^2 = 1.11$ and $M_y^2 = 1.15$ in the horizontal and vertical directions, respectively. Figure 3(d) shows the pump intensity distribution in the pre-amplifier under wave-guiding conditions, which was simulated by the ray-tracing method. The pump beam was focused into the rear part of the Ho:YAG SCF with a spot diameter of approximately 400 μm, which was well matched to the beam size of the seed laser, ranging from approximately 380 to 420 μm in the SCF. Following the initial focusing, the pump beam diverged and then was confined through total internal reflection, thus generating multiple pump gain regions along the SCF. The transverse spatial intensity distribution maintained azimuthal uniformity at different locations along the SCF, as shown in Figure 3(d), which provides favorable conditions for femtosecond pulse amplification compared with traditional rod amplifiers.

3.2. Power scaling in the multi-stage discrete Ho:YAG SCF amplifier concept

The input–output characteristics of the multi-stage Ho:YAG SCF power amplifier were first evaluated by inserting a variable attenuator into the output beam path of the pre-amplifier, enabling continuous adjustment of the injected

https://doi.org/10.1017/hpl.2025.10032 Published online by Cambridge University Press

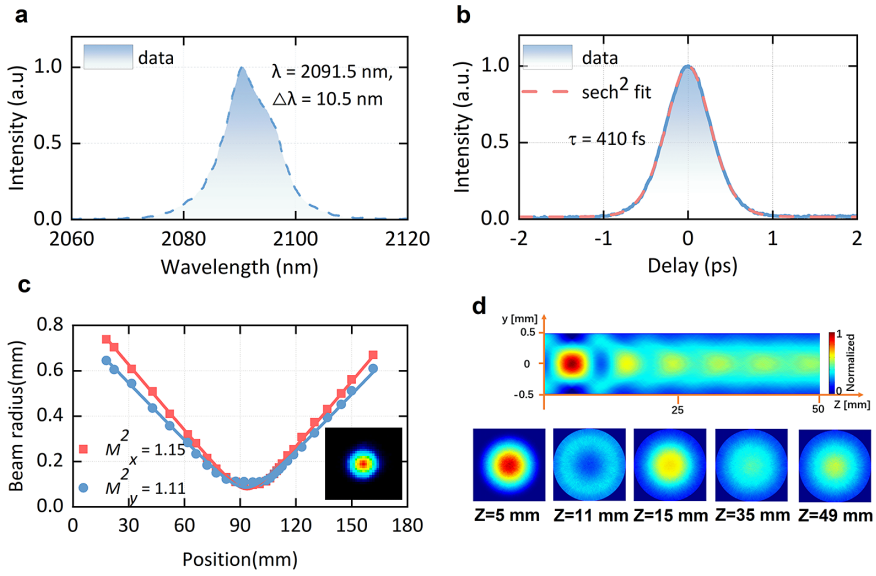

Figure 3. Performance of the Ho:YAG SCF pre-amplifier. (a) Optical spectrum and (b) autocorrelation trace measured after the pre-amplifier. (c) Beam caustics and near-field intensity profile (inset) with fitted M^2 propagation factors. (d) Simulated pump light spatial intensity distribution in the Ho:YAG SCF of the pre-amplifier pumped by the 1907 nm LD with Z indicating the distance from the input pump face.

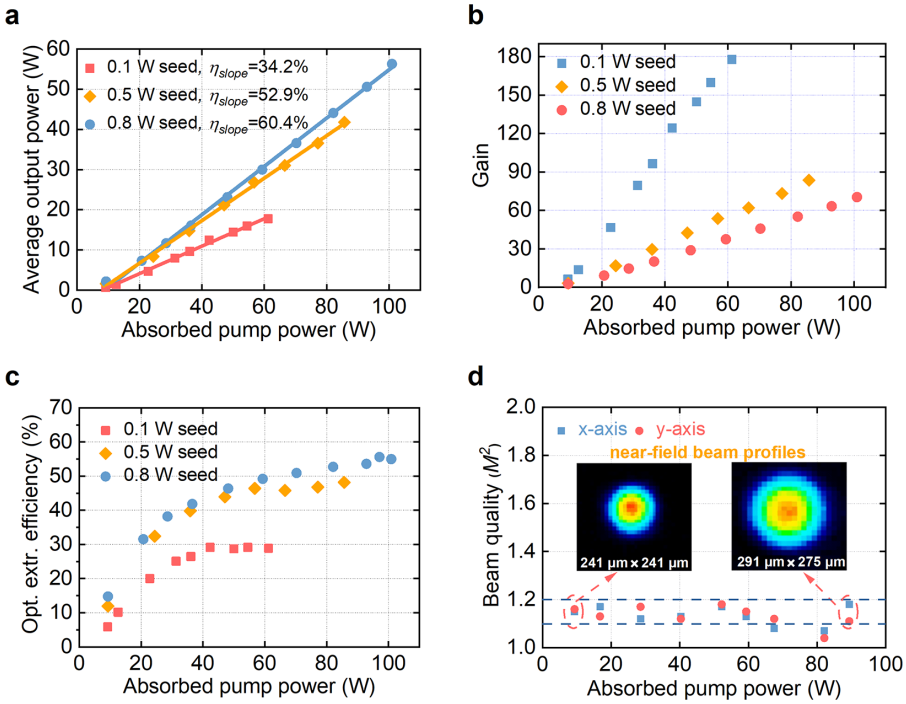

Figure 4. Input–output characteristics of the power amplifier. (a) Measured average output power, (b) net gain and (c) optical extraction efficiency versus absorbed pump power for different input levels; η_{slope}, slope efficiency with respect to absorbed pump power. (d) M^2-factors of the multi-stage Ho:YAG SCF power amplifier versus absorbed pump power measured at $P_{\text{in}} = 0.8$ W; the insets show near-field output beam profiles recorded at absorbed pump power levels of 10 W (left) and 90 W (right) with x and y designating the horizontal and vertical directions, respectively.

power without affecting other beam characteristics. The performance of the power amplifier for input average powers P_{in} of 0.1, 0.5 and 0.8 W at a constant pulse duration of approximately 410 fs is shown in Figure 4. At $P_{\text{in}} = 0.1$ W, the maximum average output level from the power amplifier reached $P_{\text{out}} = 17.8$ W at approximately 75.45 MHz with an incident pump power of 106 W, corresponding to a slope efficiency of $\eta_{\text{slope}} = 34.2\%$ with respect to the absorbed pump power, and a gain value of approximately 178. Such a remarkably high gain in the single-pass amplifier is attributed to the high-brightness pumping and the effective mode-matching in the multi-stage SCF configuration. The relatively low output power and slope efficiency at $P_{\text{in}} = 0.1$ W can be attributed to the low extraction capacity at low seed power levels. For

https://doi.org/10.1017/hpl.2025.10032 Published online by Cambridge University Press

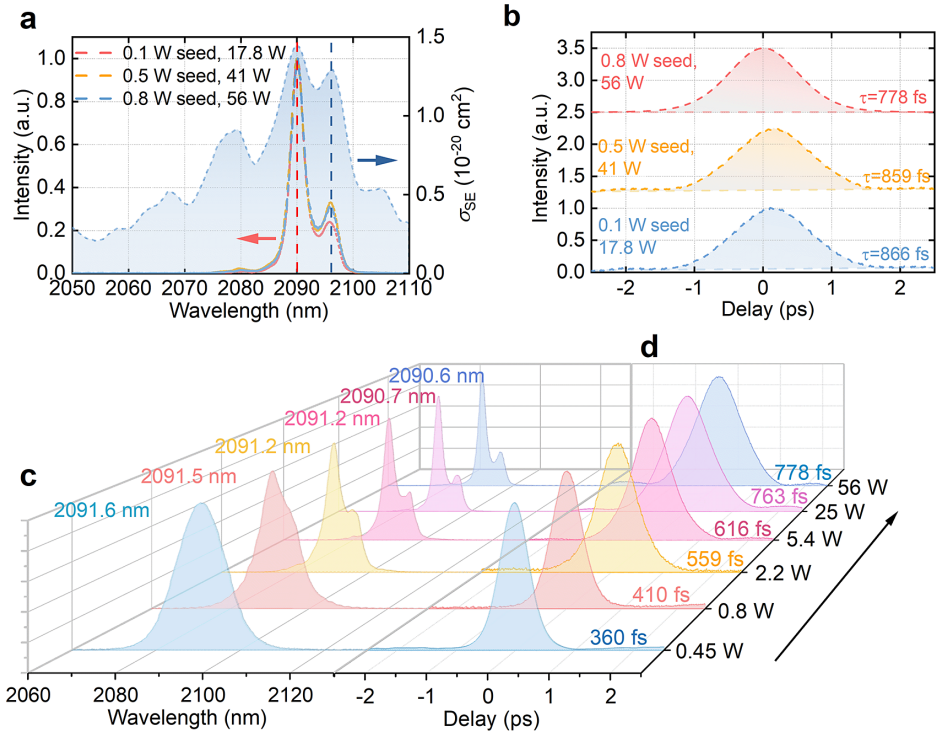

Figure 5. Spectral and temporal performance of the Ho:YAG SCF power amplifier. (a) Spectra and (b) autocorrelation traces measured at the output of the power amplifier chain at the maximum pump level for the three different seed average powers; τ is the derived pulse duration (FWHM intensity). The gray spectrum in (a) and the right-hand scale show the stimulated emission cross-section σ_{SE} of Ho:YAG. Dynamic evolution of (c) the optical spectrum and (d) the autocorrelation trace from the seed laser through the pre- and power amplifier at the maximum seed level.

$P_{in} = 0.8$ W and the same incident pump level, P_{out} reached 56.3 W with a slope efficiency of 60.4%, corresponding to a gain value of more than 70. Under these conditions, the residual pump power behind the multi-stage SCF power amplifier amounted to only approximately 5%, which leads to an optical extraction efficiency $\eta_{opt} = (P_{out} - P_{in}) / P_{abs}$ of 55.8%. To the best of our knowledge, this is the highest average power demonstrated from a 2-μm femtosecond solid-state amplifier. The absence of roll-off in the power dependence suggests that further scaling should be possible by increasing the pump power. However, the high gain of the Ho:YAG SCF (particularly at the peak emission wavelength of ~2090 nm) induces the generation of self-oscillation when the pump power is further increased, thus limiting the power scaling. This will require optimization of the SCF design, for example, enhancing signal transmittance of the end facet, tilting the device at a slight angle or cutting the end face at a small angle, which will disrupt the conditions of the self-oscillation, and further power scaling is expected. Moreover, the power scaling performance by employing single and double Ho:YAG SCFs as power amplifiers is detailed in Figures S1 and S3 in the Supplementary Material.

Moreover, the self-focusing phenomenon is most likely to occur in the final-stage SCF gain medium theoretically owing to its elevated amplification power (~56.3 W), potentially leading to an increased B-integral value. However, based on the self-focusing length (Z_f) and self-focusing critical power (P_{cr}) formulas presented in the main text, even although the pulse peak power is close to P_{cr} (~2.1 MW), the calculated $Z_f \approx 80$ mm substantially exceeds the 50-mm SCF length used experimentally. Consequently, the self-focusing phenomenon can be neglected in the discrete SCF configuration, yielding a total B-integral of approximately 0.75. For a 150-mm SCF, Z_f is significantly shorter than the gain medium length, enabling the self-focusing process to occur within the crystal. Under this condition, the calculated total B-integral is approximately 8.3, which exceeds the value under the discrete layout condition by almost a factor of 10.

For the maximum $P_{in} = 0.8$ W, the output beam quality factors at different absorbed pump powers were measured with a Spiricon charge-coupled device (CCD) camera, as shown in Figure 4(d). The beam quality factors remained below 1.2 over the entire measurement range, which confirms the spatial mode stability of the amplified beam. At an absorbed pump power of approximately 90 W, the beam quality factor was measured to be $M_x^2 = 1.18$ and $M_y^2 = 1.14$ in the horizontal and vertical directions, respectively. It can be concluded that the beam quality of the pre-amplifier is practically maintained in the power amplifier, while thermal stress-induced degradation is suppressed by direct water cooling.

https://doi.org/10.1017/hpl.2025.10032 Published online by Cambridge University Press

3.3. Dynamic evolution of the optical spectra and temporal properties

The output spectra from the power amplifier under maximum pump power were similar for the three injected power levels of 0.1, 0.5 and 0.8 W, corresponding to pulse durations of 778, 859 and 866 fs, respectively; see Figures 5(a) and 5(b). To analyze the spectral and temporal evolution, the measured spectra and pulse durations are summarized in Figures 5(c) and 5(d) for all stages (including those of the mode-locked laser and the pre-amplifier). Compared with the spectrum of the seed laser centered at approximately 2091.6 nm, the FWHM of the spectra gradually decreased, and the central wavelength shifted to approximately 2090.6 nm. Meanwhile, a weaker spectral peak appeared at approximately 2096 nm, which correlates with the gain spectrum of Ho:YAG (see Figure 5(a)). The spectrum of the power amplifier at the average power of approximately 56 W shows no indication of amplified spontaneous emission (ASE) or nonlinear effects, which highlights the main advantages of the SCF, namely, high overall gain and nonlinear effects suppression. To overcome the gain narrowing in the power amplifier, an effective solution in future work would be initial spectral shaping with suppressed peak intensity of the seed light[15,47].

The autocorrelation trace at maximum output power of the power amplifier indicates a pulse duration of 778 fs without any significant pulse distortion. Remarkably, the ultrashort pulse was amplified up to 0.75 μJ pulse energy and 0.84 MW peak power without a stretcher–compressor configuration. Such high performance of the ultrafast amplifier (i.e., high efficiency, high average power and good beam quality) obviously benefited from the long gain region, the nonlinear effects suppression and the large surface-to-volume ratio of the multi-stage Ho:YAG SCF amplification system. Similarly, the dynamic evolution of the optical spectra and temporal properties are shown in Figures S2 and S4 in the Supplementary Material.

4. Conclusions

In conclusion, we have experimentally demonstrated a compact, high-performance multi-stage SCF amplifier for direct amplification of femtosecond pulses at 2 μm without pulse picking, stretching or compression. The multiple SCFs in the power amplifier were designed to lengthen the gain region and provide a uniform heat distribution, which was instrumental in achieving a maximum average power of 56.3 W at 75.45 MHz with a slope efficiency of 60.4% and near-diffraction-limited beam quality ($M^2 < 1.2$). To the best of our knowledge, this laser amplifier has produced the record average power from a direct femtosecond amplification system, and also the highest value among femtosecond solid-state lasers and parametric amplifiers in the 2-μm spectral region[15,18,19,34,37,48–58]; see Figure 6. Simultaneously, it is the only system operating at high repetition rates apart from the long-cavity thin-disk oscillator[37] mode-locked at 23.5 MHz albeit with more than 1 ps pulse duration. These results show that the developed multi-stage SCF amplifier is an attractive alternative to multi-pass or regenerative amplifiers and at the same time avoids the disadvantages of OPCPA systems (e.g., complexity and price, low efficiency, strict synchronization with pump pulses).

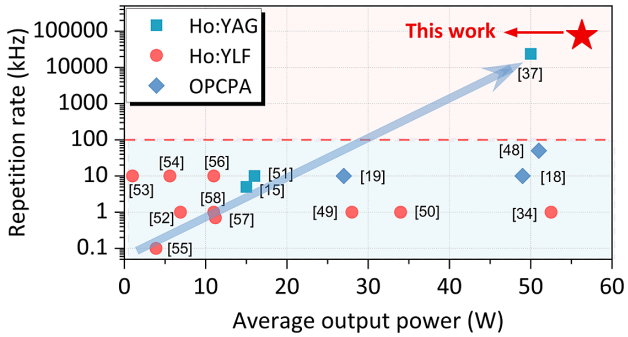

Figure 6. Overview of 2-μm ultrafast amplifiers based on Ho-doped bulk gain media and OPCPA[15,18,19,34,37,48-58]. Note that the results of direct amplification of femtosecond pulses in conventional fibers are not described here due to their much lower power level.

Acknowledgements

This work was financially supported by the National Natural Science Foundation of China (Grant Nos. 62475106, U23A20558, 52025021 and 52032009), the Natural Science Foundation of Shandong Province, China (Grant No. ZR2024ZD16) and the Foundation of the National Key Laboratory of Plasma Physics (Grant No. 6142A04230301). Y. Zhao acknowledges financial support from the Qilu Young Scholars Program of Shandong University.

Supplementary material

The supplementary material for this article can be found at http://doi.org/10.1017/hpl.2025.10032.

References

1. M. Gebhardt, T. Heuermann, R. Klas, C. Liu, A. Kirsche, M. Lenski, Z. Wang, C. Gaida, J. E. Antonio-Lopez, A. Schülzgen, R. Amezcua-Correa, J. Rothhardt, and J. Limpert, Light Sci. Appl. **10**, 36 (2021).
2. T. Popmintchev, M.-C. Chen, D. Popmintchev, P. Arpin, S. Brown, S. Ališauskas, G. Andriukaitis, T. Balčiunas, O. D. Mücke, A. Pugzlys, A. Baltuška, B. Shim, S. E. Schrauth, A. Gaeta, C. Hernández-García, L. Plaja, A. Becker, A. Jaron-Becker, M. M. Murnane, and H. C. Kapteyn, Science **336**, 1287 (2012).
3. E. Sistrunk, D. A. Alessi, A. Bayramian, K. Chesnut, A. Erlandson, T. C. Galvin, D. Gibson, H. Nguyen, B. Reagan, K. Schaffers, C. W. Siders, T. Spinka, and C. Haefner, Proc. SPIE **11034**, 1103407 (2019).
4. V. Petrov, Prog. Quant. Electron. **42**, 1 (2015).
5. R. R. Gattass and E. Mazur, Nat. Photonics **2**, 219 (2008).
6. C. Kerse, H. Kalaycıoğlu, P. Elahi, B. Çetin, D. K. Kesim, Ö. Akçaalan, S. Yavaş, M. D. Aşık, B. Öktem, H. Hoogland, R. Holzwarth, and F. Ö. Ilday, Nature **537**, 84 (2016).
7. G. Steinmeyer, D. H. Sutter, L. Gallmann, N. Matuschek, and U. Keller, Science **286**, 1507 (1999).
8. M. T. Sohail, B. Li, C. Guo, M. Younis, M. Shareef, M. Abdullah, and P. Yan, Adv. Mater. Technol. **9**, 2400496 (2024).
9. D. C. Kirsch, S. Chen, R. Sidharthan, Y. Chen, S. Yoo, and M. Chernysheva, J. Appl. Phys. **128**, 180906 (2020).
10. Z. Chang, L. Fang, V. Fedorov, C. Geiger, S. Ghimire, C. Heide, N. Ishii, J. Itatani, C. Joshi, Y. Kobayashi, P. Kumar, A. Marra, S. Mirov, I. Petrushina, M. Polyanskiy, D. A. Reis, S. Tochitsky, S. Vasilyev, L. Wang, Y. Wu, and F. Zhou, Adv. Opt. Photon. **14**, 652 (2022).
11. Z. Li, Y. Leng, and R. Li, Laser Photonics Rev. **17**, 2100705 (2023).
12. J. Rothhardt, S. Hädrich, J. Delagnes, E. Cormier, and J. Limpert, Laser Photonics Rev. **11**, 1700043 (2017).
13. D. Strickland and G. Mourou, Opt. Commun. **55**, 447 (1985).
14. J. Pupeikis, P. A. Chevreuil, N. Bigler, L. Gallmann, C. R. Phillips, and U. Keller, Optica **7**, 168 (2020).
15. P. Malevich, G. Andriukaitis, T. Flöry, A. J. Verhoef, A. Fernández, S. Ališauskas, A. Pugžlys, A. Baltuška, L. H. Tan, C. F. Chua, and P. B. Phua, Opt. Lett. **38**, 2746 (2013).
16. Z. Wang, T. Heuermann, M. Gebhardt, M. Lenski, P. Gierschke, R. Klas, J. Rothhardt, C. Jauregui, and J. Limpert, Opt. Lett. **48**, 2647 (2023).
17. K.-H. Hong, C.-J. Lai, J. P. Siqueira, P. Krogen, J. Moses, C.-L. Chang, G. J. Stein, L. E. Zapata, and F. X. Kärtner, Opt. Lett. **39**, 3145 (2014).
18. M. F. Seeger, D. Kammerer, J. Blöchl, M. Neuhaus, V. Pervak, T. Nubbemeyer, and M. F. Kling, Opt. Express **31**, 24821 (2023).
19. T. Feng, A. Heilmann, M. Bock, L. Ehrentraut, T. Witting, H. Yu, H. Stiel, S. Eisebitt, and M. Schnürer, Opt. Express **28**, 8724 (2020).
20. L. von Grafenstein, M. Bock, D. Ueberschaer, E. Escoto, A. Koç, K. Zawilski, P. Schunemann, U. Griebner, and T. Elsaesser, Opt. Lett. **45**, 5998 (2020).
21. M. Galletti, P. Oliveira, M. Galimberti, M. Ahmad, G. Archipovaite, N. Booth, E. Dilworth, A. Frackiewicz, T. Winstone, I. Musgrave, and C. Hernandez-Gomez, High Power Laser Sci. Eng. **8**, e31 (2020).
22. S. Klingebiel, C. Wandt, C. Skrobol, I. Ahmad, S. A. Trushin, Z. Major, F. Krausz, and S. Karsch, Opt. Express **19**, 5357 (2011).
23. D. J. Richardson, J. Nilsson, and W. A. Clarkson, J. Opt. Soc. Am. B **27**, B63 (2010).
24. J. Zuo and X. Lin, Laser Photonics Rev. **16**, 2100741 (2022).
25. J. C. Knight, Nature **424**, 847 (2003).
26. J. M. Dudley and J. R. Taylor, Nat. Photonics **3**, 85 (2009).
27. C. Gaida, M. Gebhardt, T. Heuermann, F. Stutzki, C. Jauregui, and J. Limpert, Opt. Lett. **43**, 5853 (2018).
28. F. Stutzki, C. Gaida, M. Gebhardt, F. Jansen, C. Jauregui, J. Limpert, and A. Tünnermann, Opt. Lett. **40**, 9 (2015).
29. M. Baumgartl, F. Jansen, F. Stutzki, C. Jauregui, B. Ortaç, J. Limpert, and A. Tünnermann, Opt. Lett. **36**, 244 (2011).
30. S. Février, B. Beaudou, and P. Viale, Opt. Express **18**, 5142 (2010).
31. C. Gaida, M. Gebhardt, F. Stutzki, C. Jauregui, J. Limpert, and A. Tünnermann, Opt. Lett. **41**, 4130 (2016).
32. T. Heuermann, Z. Wang, M. Lenski, M. Gebhardt, C. Gaida, M. Abdelaal, J. Buldt, M. Müller, A. Klenke, and J. Limpert, Opt. Lett. **47**, 3095 (2022).
33. L. von Grafenstein, M. Bock, D. Ueberschaer, U. Griebner, and T. Elsaesser, Opt. Lett. **41**, 4668 (2016).
34. L. von Grafenstein, M. Bock, D. Ueberschaer, A. Koç, U. Griebner, and T. Elsaesser, Opt. Lett. **45**, 3836 (2020).
35. J. Drs, J. Fischer, N. Modsching, F. Labaye, M. Müller, V. J. Wittwer, and T. Südmeyer, Laser Photonics Rev. **17**, 2200258 (2023).
36. S. Goncharov, K. Fritsch, and O. Pronin, Opt. Express **31**, 25970 (2023).
37. S. Tomilov, Y. Wang, M. Hoffmann, J. Heidrich, M. Golling, U. Keller, and C. J. Saraceno, Opt. Express **30**, 27662 (2022).
38. X. Délen, A. Aubourg, L. Deyra, F. Lesparre, I. Martial, J. Didierjean, F. Balembois, and P. Georges, Proc. SPIE **9342**, 934202 (2015).
39. J. Liu, J. Dong, Y. Wang, J. Guo, Y. Xue, J. Xu, Y. Zhao, X. Xu, H. Yu, Z. Wang, X. Xu, W. Chen, and V. Petrov, Opt. Lett. **46**, 4454 (2021).
40. Y. Zhao, C. Zheng, Z. Huang, Q. Gao, J. Dong, K. Tian, Z. Yang, W. Chen, and V. Petrov, Laser Photonics Rev. **16**, 2200503 (2022).
41. F. Beirow, M. Eckerle, T. Graf, and M. A. Ahmed, Appl. Phys. B **126**, 148 (2020).
42. X. Délen, Y. Zaouter, I. Martial, N. Aubry, J. Didierjean, C. Hönninger, E. Mottay, F. Balembois, and P. Georges, Opt. Lett. **38**, 109 (2013).
43. W. Koechner, *Solid-state Laser Engineering* (Springer, Berlin Heidelberg, 2013), p. 202.
44. C.-H. Lu, Y.-J. Tsou, H.-Y. Chen, B.-H. Chen, Y.-C. Cheng, S.-D. Yang, M.-C. Chen, C.-C. Hsu, and A. H. Kung, Optica **1**, 400 (2014).
45. N. Zhang, P. Wang, B. Chen, Z. Wang, S. Liu, Y. Zhao, Z. Jia, B. Zhang, and Z. Sun, Appl. Phys. B **128**, 128 (2022).
46. N. Zhang, Q. Song, J. Zhou, J. Liu, S. Liu, H. Zhang, X. Xu, Y. Xue, J. Xu, W. Chen, Y. Zhao, U. Griebner, and V. Petrov, Opt. Lett. **48**, 510 (2023).
47. P. Malevich, T. Kanai, H. Hoogland, R. Holzwarth, A. Baltuška, and A. Pugžlys, Opt. Lett. **41**, 930 (2016).
48. P. Gierschke, C. Grebing, M. Abdelaal, M. Lenski, J. Buldt, Z. Wang, T. Heuermann, M. Mueller, M. Gebhardt, J. Rothhardt, and J. Limpert, Opt. Lett. **47**, 3511 (2022).
49. K. Murari, F. Zhou, Y. Yin, Y. Wu, B. Weaver, T. Avni, E. Larsen, and Z. Chang, Appl. Phys. Lett. **117**, 141102 (2020).
50. L. von Grafenstein, M. Bock, D. Ueberschaer, U. Griebner, and T. Elsaesser, Opt. Express **23**, 33142 (2015).
51. I. Astrauskas, B. Považay, A. Baltuška, and A. Pugžlys, Opt. Laser Technol. **133**, 106535 (2021).
52. P. Kroetz, A. Ruehl, G. Chatterjee, A.-L. Calendron, K. Murari, H. Cankaya, P. Li, F. X. Kärtner, I. Hartl, and R. J. Dwayne Miller, Opt. Lett. **40**, 5427 (2015).
53. M. Hinkelmann, D. Wandt, U. Morgner, J. Neumann, and D. Kracht, Proc. SPIE **10511**, 1051109 (2018).

https://doi.org/10.1017/hpl.2025.10032 Published online by Cambridge University Press

54. M. Hinkelmann, D. Wandt, U. Morgner, J. Neumann, and D. Kracht, Opt. Express **26**, 18125 (2018).
55. M. Hemmer, D. Sánchez, M. Jelínek, V. Smirnov, H. Jelinkova, V. Kubeček, and J. Biegert, Opt. Lett. **40**, 451 (2015).
56. L. von Grafenstein, M. Bock, U. Griebner, and T. Elsaesser, Opt. Express **23**, 14744 (2015).
57. L. von Grafenstein, M. Bock, G. Steinmeyer, U. Griebner, and T. Elsaesser, Laser Photonics Rev. **10**, 123 (2016).
58. D. Alex, Proc. SPIE **8599**, 85990B (2013).

https://doi.org/10.1017/hpl.2025.10032 Published online by Cambridge University Press